Supplemental Information for

Therapeutic Antibodies to Ganglioside GD2 Evolved from Highly Selective Germline Antibodies

Eric Sterner[1], Megan L. Peach[2], Marc C. Nicklaus[1], and Jeffrey C. Gildersleeve [1*]

1. Chemical Biology Laboratory, Center for Cancer Research, National Cancer Institute, Frederick, MD, 21702
2. Basic Science Program, Chemical Biology Laboratory, Leidos Biomedical Inc., Frederick National Laboratory for Cancer Research, Frederick, MD 21702

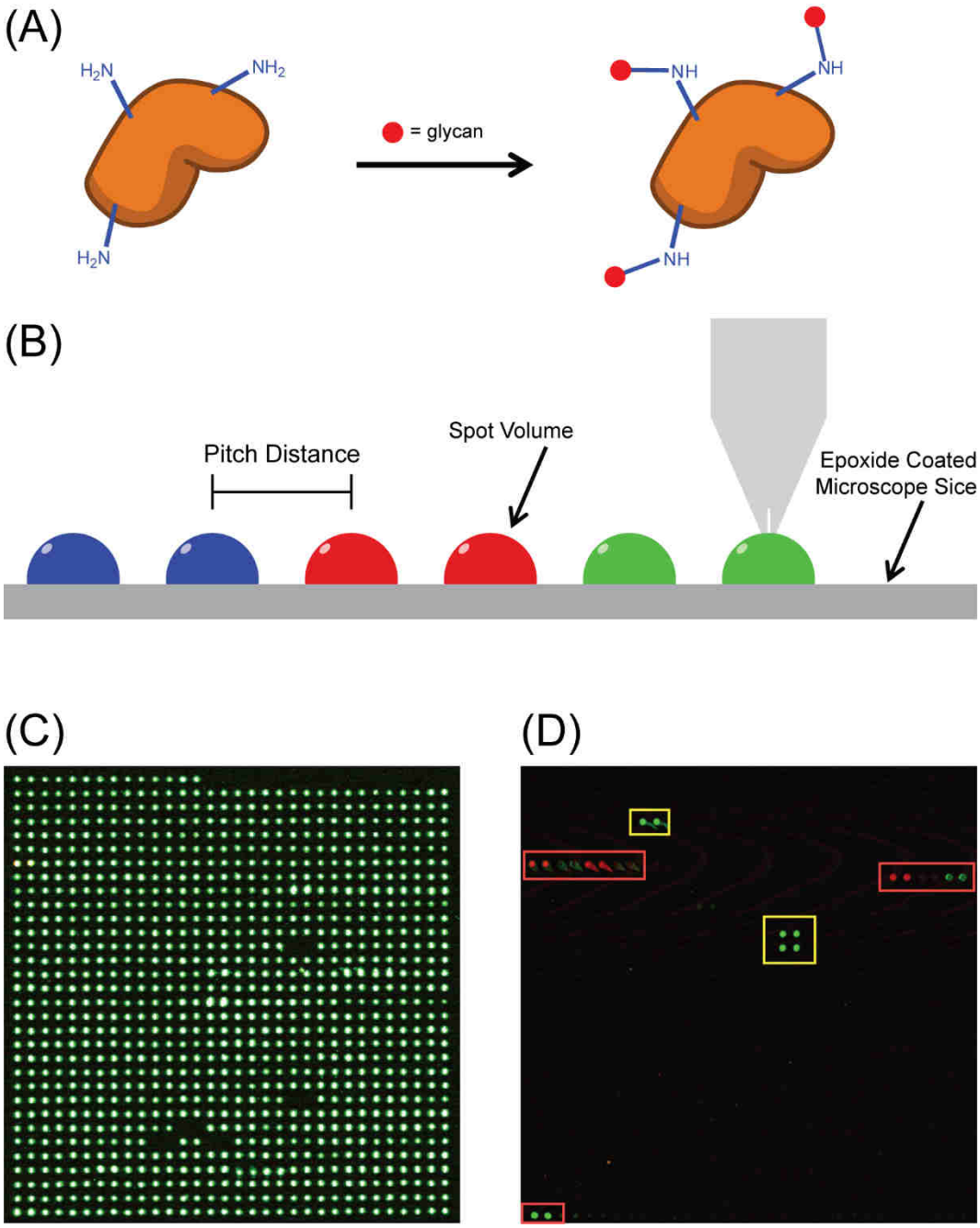

Figure S1, related to Figure 3: Cartoon schematic of neoglycoprotein synthesis and printing and example images of the glycan array. (a) Glycans are covalently immobilized on carrier proteins, typically BSA or HSA, through free amines of lysine residues as previously described (Zhang and Gildersleeve, 2012). (b) Neoglycoproteins are immobilized on epoxide-coated microscope slides using robotic, contact-spotting arrayer. Slide quality is controlled based on spotting volume and distance between spots (pitch distance) (Campbell, et al., 2010). (c) Prescan images of the slides were taken to evaluate slide quality. Missing spots are flagged and excluded from further analysis. (d) Following experimentation, slides were scanned to evaluate antibody binding. The image in panel B is representative of germline 3F8 binding on the glycan array. Spots within yellow boxes represent GD2-neoglycoprotein spots. Spots within red boxes are control spots, such as human IgG, human IgM, and Cy3.

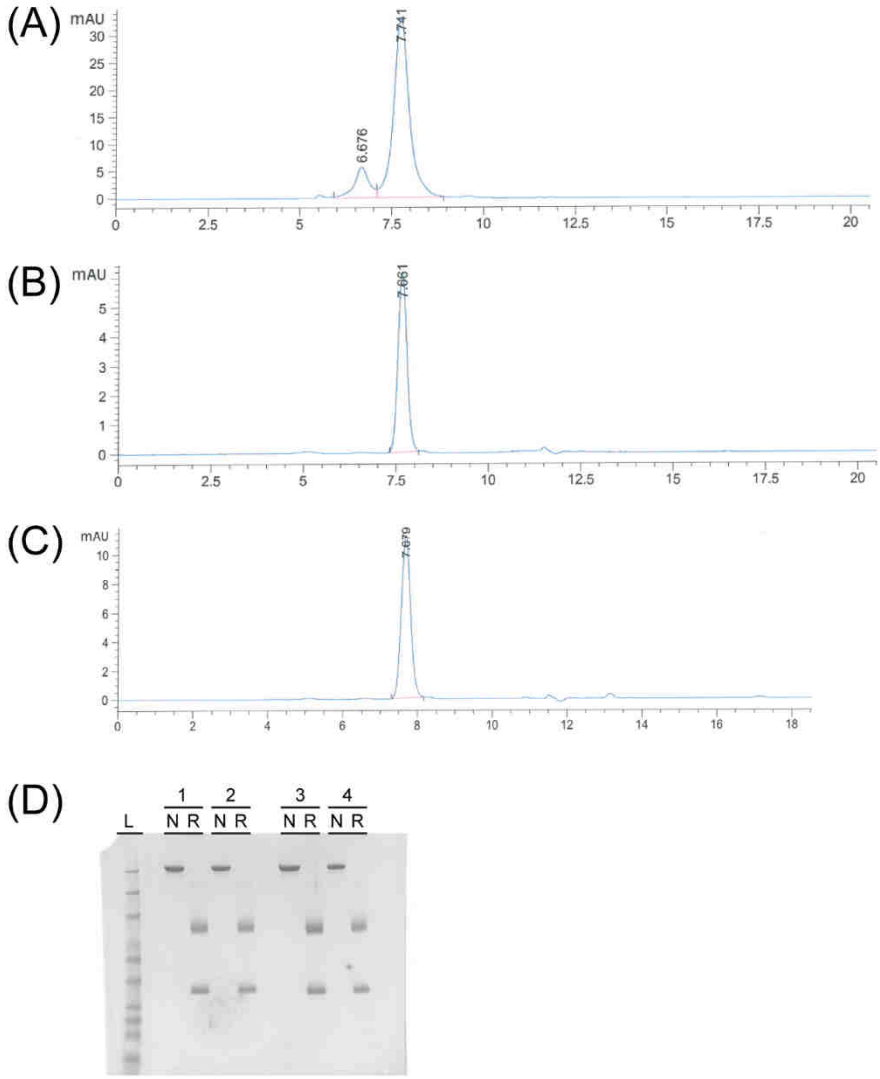

Figure S2, related to figure 3: Size exclusion chromatography and polyacrylamide gel electrophoresis analyses. (a-c) Samples were run on a TOSOH TSKgel G3000SWxl column to determine the purity of antibodies produced in cell culture. (a) Pooled human IgG was run to determine expected elution times. (b) Mature and (c) germline 3F8 antibodies eluted at the expected time point of ~7.7 mins. No significant impurities were observed in the chromatograms. A peak representative of dimeric IgG, observed at 6.7 mins in the human IgG chromatogram, is noticably absent in the mature and germline 3F8 antibody chromatograms. (d) Anti-GD2 antibodies purified by affinity chromatography were run in native (N) and reduced (R) formats on a Bolt 4-12% Bis-Tris gel (1x MES SDS running buffer, 150V, 45 mins). Anti-GD2 samples: (1) Affinity mature 3F8, (2) Germline 3F8, (3) Affinity mature 14.18, and (4) Germline 14.18. Control ladder (L) run in leftmost well.

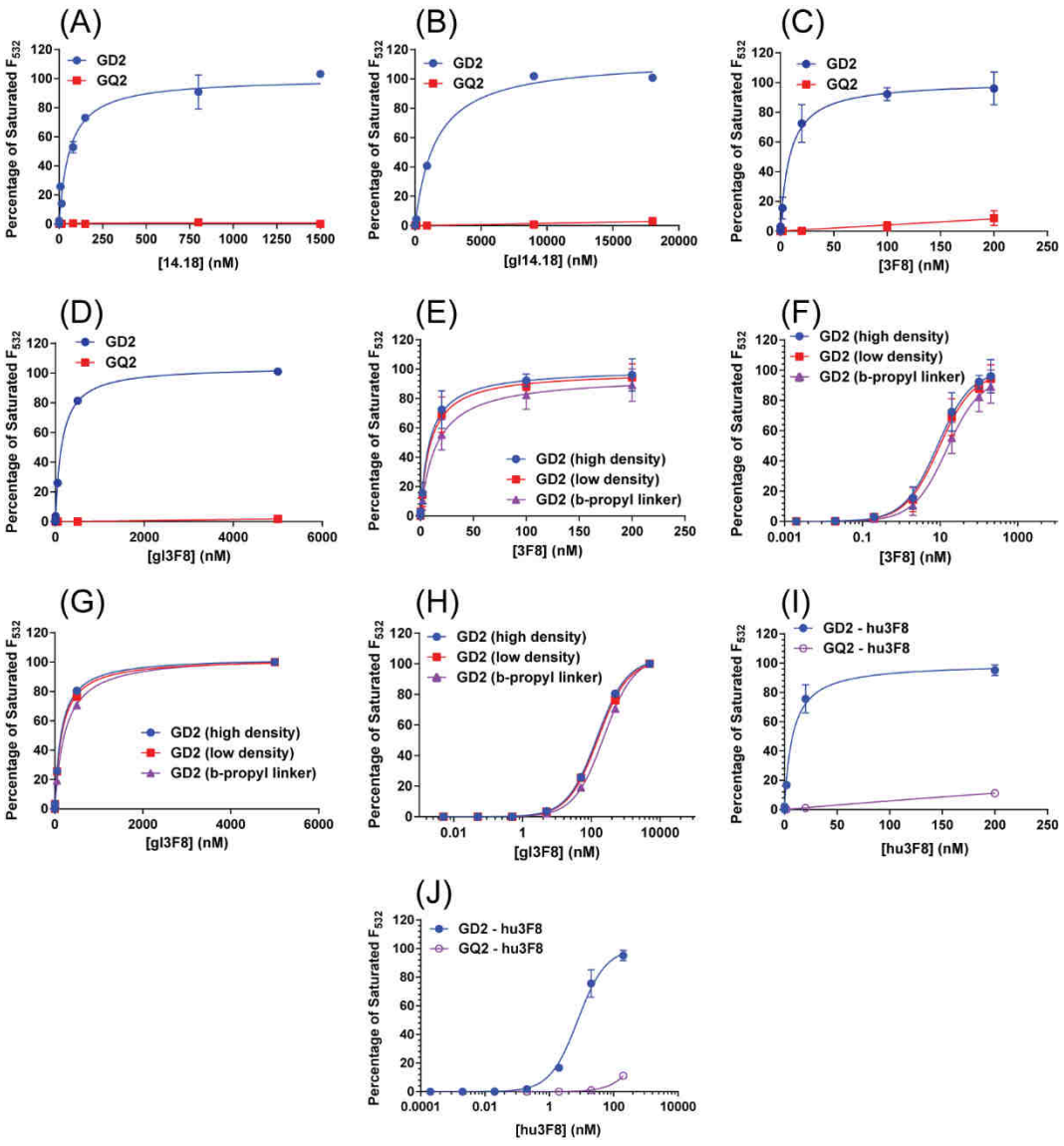

Figure S3, related to Figure 3: Curves of dose response data for anti-GD2 antibodies. (a-d) This data is a linear re-plotting of the data in Figure 3 to clearly illustrate antibody-spot saturation. (a) Affinity mature 14.18 antibody, (b) germline 14.18 antibody, (c) affinity mature 3F8 antibody, and (d) germline 3F8 antibody. (e-h) Variations in GD2 density per carrier protein does not affect apparent dissociation constants. Three distinct variations of GD2 presentation are present on the A503 glycan array. Two of these variations are high and low density GD2, represented by blue circles and red squares respectively. By MALDI analysis, the average GD2 conjugation per carrier protein was 10:1 the high density neoglycoprotein and 4:1 for the low density variant. The third variant differs in the conjugation linker (b-propyl); these neoglycoproteins are represented by the purple triangles. The difference in the calculated apparent dissociation constant was nominal for all antibodies tested (summarized in Table S2). (e-f) Mature 3F8 antibody: (e) Linear and (f) log-10 dose response curves. (g-h) Germline 3F8 antibody: (g) linear and (h) log-10 dose response curves. The high density GD2 (blue circles) data are replottings of Figure 3 and Figure S2 data for comparative purposes. (i-j) Humanized 3F8 antibody binds GD2 specifically. The amino acid alignment of this humanized variant was originally described by Cheung, et al., 2012. The humanized 3F8 variant maintains high affinity and good specificity for the GD2 antigen; (i) linear and (j) log-10 dose response plots for the humanized 3F8 antibody. Data are represented as mean ± standard deviation for a minimum of 2 array spots.

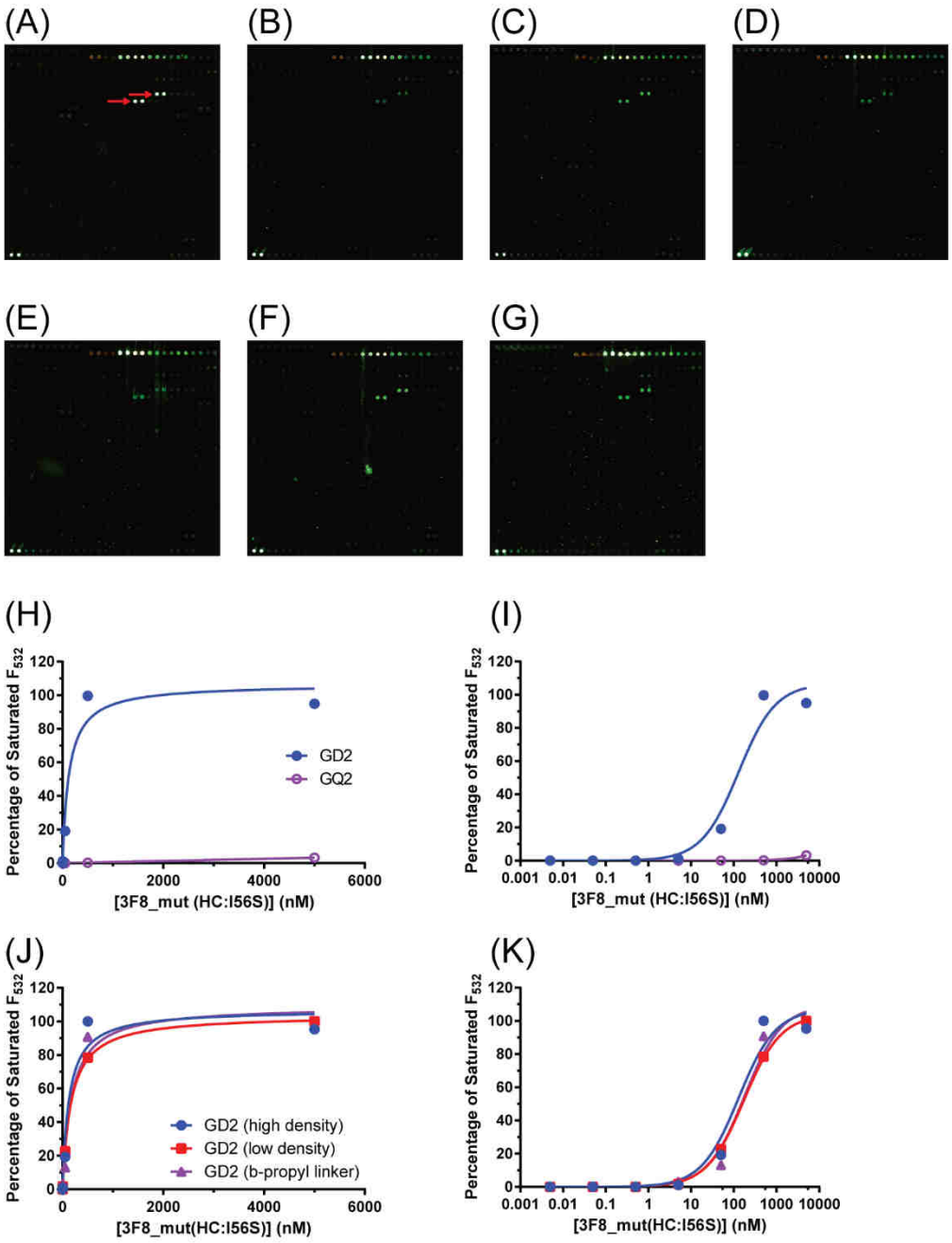

Figure S4, related to Figure 3: 3F8 structures representative of a single reversion in maturation status. Concentrated supernatants of HEK293 cell lines producing (a) mature 3F8 antibody (red arrows = GD2-neoglycoprotein replicates) and (b-g) single germline-reversion mutants. Array images are of (b) Light Chain:T34A, (c) Light Chain:S50Y, (d) Heavy Chain:V29L, (e) Heavy Chain:N31S, (f) Heavy Chain:I56S, and (g) Heavy Chain:L106M. 406-component arrays were used for these simple binding experiments, as opposed to the 503-component arrays for the determination of apparent dissociation constants ($K_{D,app}$). One 3F8 germline-reversion mutant (ch3F8_mut(HC:I56S)) was selected for extended dose-response. The mutant 3F8 maintains good specificity for the GD2 antigen and has affinity comparable to the germline 3F8 antibody; (h) linear and (i) log-10 dose response plots for the ch3F8_mut(HC:I56S) antibody. Similarly to other tested antibodies, apparent K_D values are mostly unaffected by density or linker conjugation; (j) linear and (k) log-10 plots. Data are represented as mean ± standard deviation for a minimum of 2 array spots.

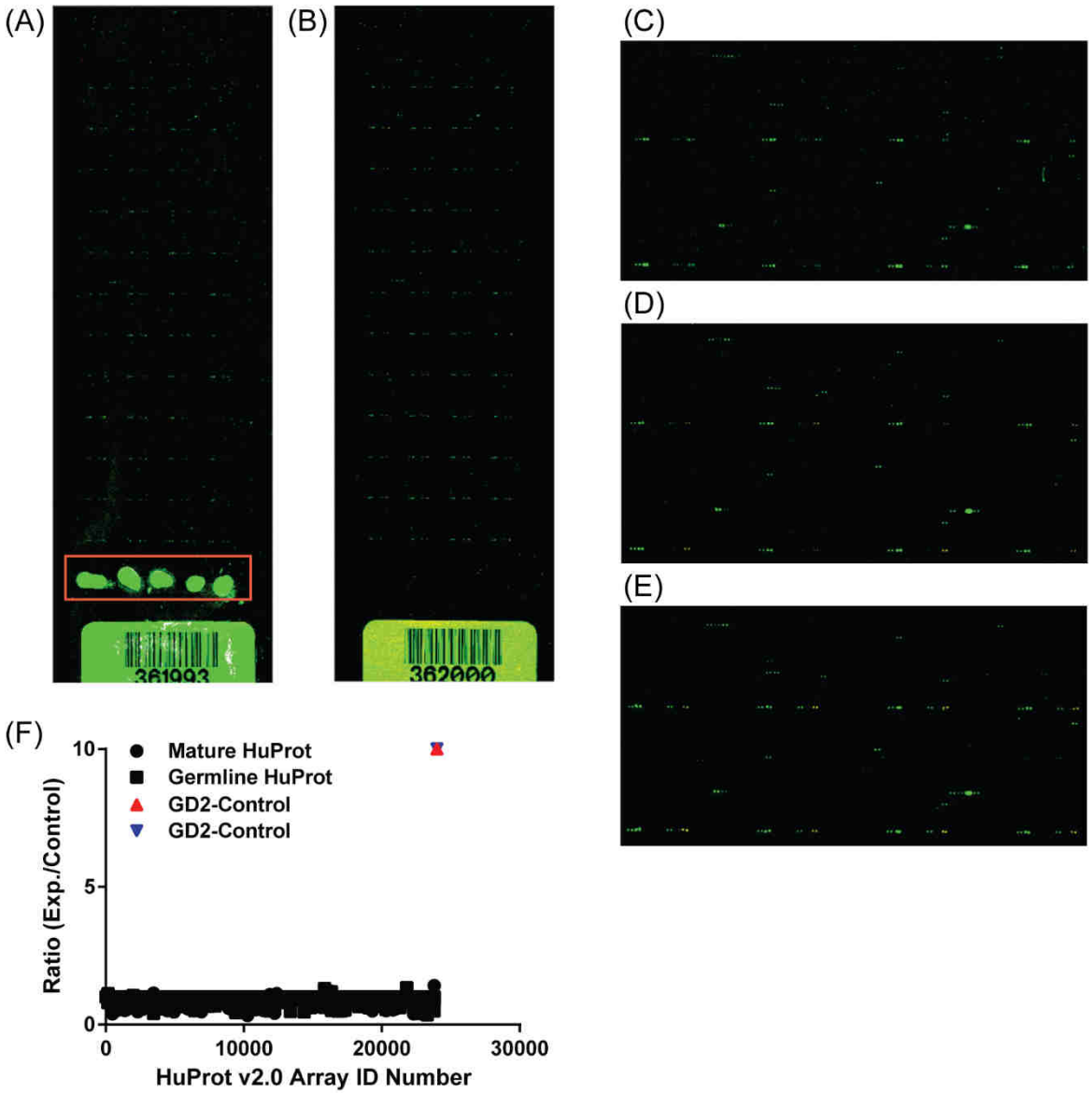

Figure S5, related to Figure 3: (a-b) Full images of the HuProt array experiments. (a) Experiments with 3F8 demonstrated no unique binding events compared to the (b) control, secondary antibody only slide. The 3F8 antibody was able to bind the manually printed GD2-neoglycoprotein (red box). Secondary alone was incapable of binding the GD2-neoglycoprotein, consistent with the glycan array. (c-e) 2x4 subarray images from 3 unique experiments. (c) Affinity mature 3F8, (d) germline 3F8, and (e) no anti-GD2 antibody, secondary only. (f) 3F8 antibodies were incapable of binding to target proteins on the HuProt v2.0 array. Differences between the test slides and the control slide (no 3F8 antibody) were negligible and no spots were identified as unique to the test 3F8 slides. Antibodies were reactive with the manually printed GD2 control spots added to the bottom of all slides (red and blue triangles). Values noticeably above baseline (orange circle) are the result of gal file resizing issues that could not be resolved; corresponding spots on control slide were too small to analyze properly. All experimental analyses were done in duplicate; two array experiments per 3F8 antibody (4 slides total) and two control (secondary only) slides.

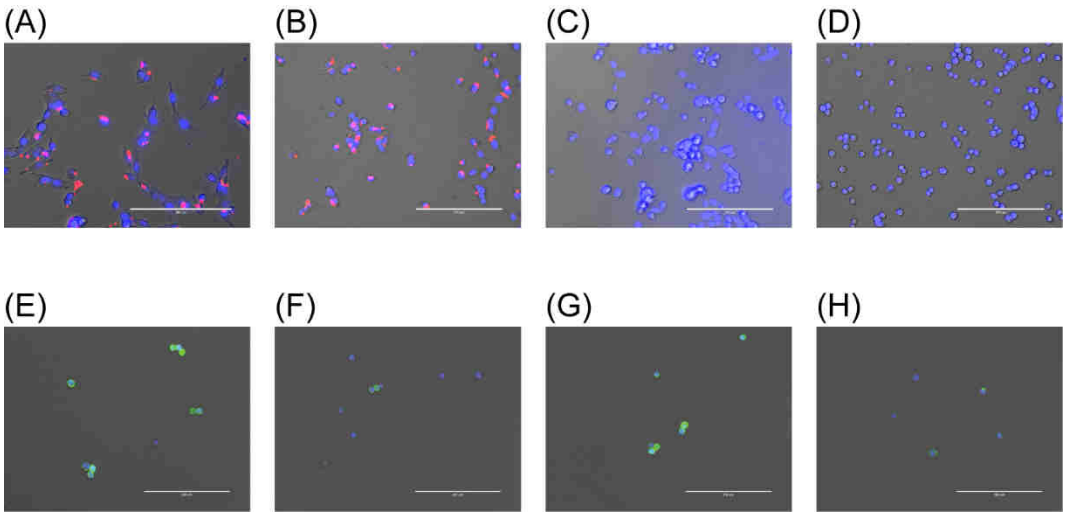

Figure S6, related to Figure 4: (a-d) Live cell binding experiments of mature and germline 3F8 antibodies with the M14 melanoma and SW620 colorectal cancer cell lines (Scale bars, 200 µm). (a-b) The anti-GD2 antibodies were capable of binding the GD2-positive M14 melanoma cell line. 3F8 antibody binding was detected by the addition of DyLight™649-conjugated goat anti-human IgG secondary reagent. (c) The secondary reagent alone was incapable of binding the M14 cell line. (d) The 3F8 antibody was also incapable of binding the colorectal cancer cell line SW620. (e-h) Fixed, non-adherent cell binding experiments of anti-GD2 antibodies with the M14 melanoma and SW620 colorectal cancer cell lines (Scale bars, 200 µm). The (e) mature and (f) germline 3F8 antibodies were capable of binding the GD2-positive M14 melanoma cell line. The (g) mature and (h) germline 14.18 antibodies were also capable of binding. Anti-GD2 antibody binding was detected by the addition of Cy2-conjugated donkey anti-human IgG secondary antibody. Anti-GD2 antibodies were incapable of binding the SW620 colorectal cancer cell line (Table S3). The integrity of the colorectal cancer cell line was validated using anti-blood group A antibody HE-195 and the addition of DyLight649 conjugated goat anti-mouse IgM secondary (Table S3). HE-195 was incapable of binding M14 melanoma.

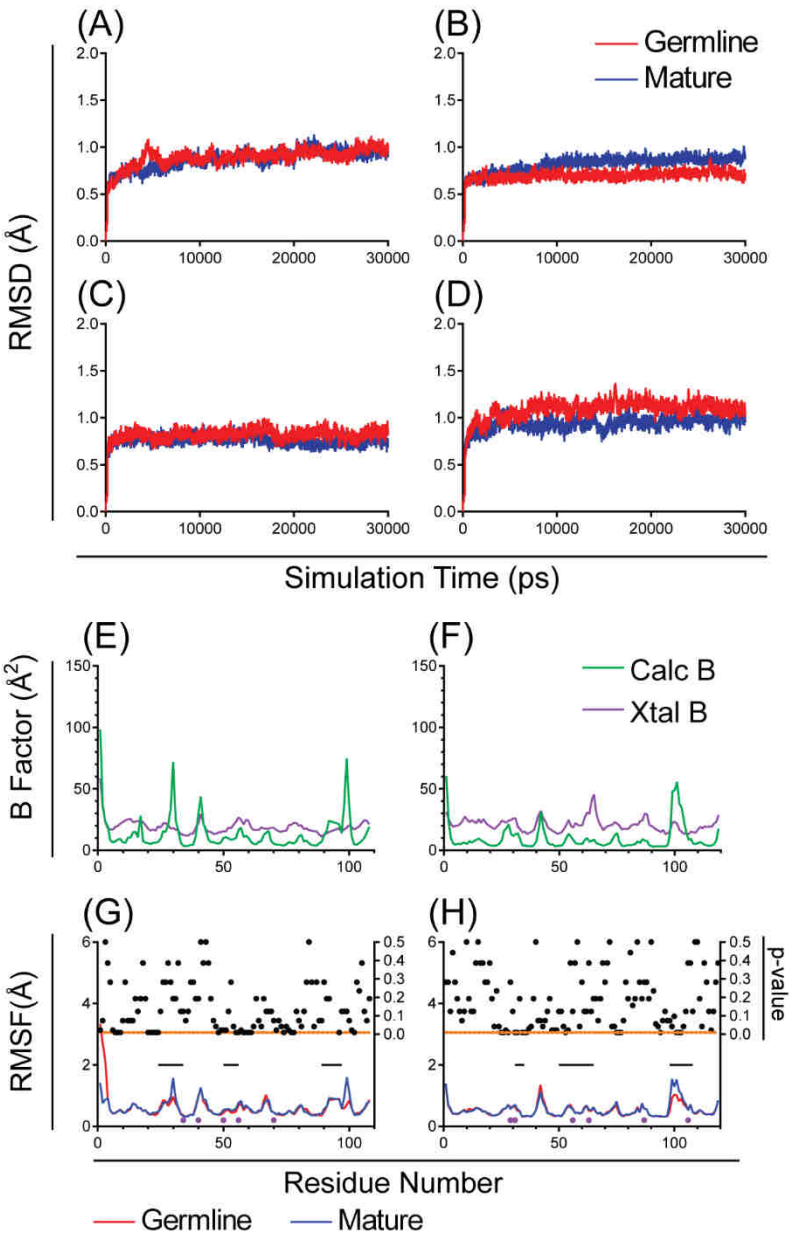

Figure S7, related to Figure 5: Molecular dynamics simulations data of mature 3F8 Fab and its germline homologue. (a-d) The germline and mature 3F8 Fabs were energy minimized, then four copies of each structure were setup and initialized with random starting velocities. The RMSD(Å) of the (a) variable light chain, (b) variable heavy chain, (c) constant light chain, and (d) constant heavy chain regions were observed over the 30 ns simulation time. Each plot above is representative of the average RMSD(Å) from four unique simulations. (a-b) Comparison of the calculated (green) and crystallographic (purple) B factors of the mature 3F8 antibody. Regions of increased and decreased flexibility in the (a) light chain and (b) heavy chain are qualitatively reproduced. (c-d) RMS-fluctuation calculations of the mature (blue) and germline (red) Fab variable domain simulations for the (c) light chain variable and (d) heavy chain variable regions. RMSF(Å) is plotted on the left y-axis with residue number plotted on the x-axis. The location of germline-to-affinity mature mutations are noted by the purple circles below the plots; black bars above the plots indicate complementary determining regions (CDRs). P-values for the statistical significance of differences in RMSF between mature and germline structures are plotted as black circles on the right y-axis. A reference p-value of 0.01 is marked by the horizontal, orange-dashed line.

Table S1, related to Experimental Procedures: Primers used in colony polymerase chain reaction (colony PCR) experimentations.

Primer Name	Primer Sequence (5'-3')	T_M (°C)	PCR Product Length (base pairs; empty vector)
pFuse2-CLIg-hk_fwd	TTTGCCTGACCCTGCTTGCT	62.7	242
pFuse2-CLIg-hk_rev	TCCACTGTACTTTGGCCTCTCT	60.8	
pFuse-CHIg-hG1_fwd	CTGACCCTGCTTGCTCAACT	60.3	390
pFuse-CHIg-hG1_rev	GTGTTGCTGGGCTTGTGATT	59.3	

Table S2, related to Figure 3: Apparent dissociations constants of anti-GD2 antibodies are unaffected by variations in antigen density. $K_{D,App}$ for germline 14.18 (gl_14.18) and GD2 (b-propyl linker) interactions was not determined (N.D.).

	Apparent Dissociation Constants: $K_{D,app}$ (nM)		
Antibody	**GD2 (high density)**	**GD2 (low density)**	**GD2 (b-propyl linker)**
ch3F8	8.5	9.3	14
gl_ch3F8	146	160	233
hu3F8	7.7	8.6	15
ch3F8_mut (H:I56S)	128	170	178
ch14.18	60	75	71
gl_ch14.18	1600	1400	N.D.

Table S3, related to Figure 4: Summary of fluorescence-activated cell sorting (FACS) analyses for germline and affinity mature 3F8 antibodies. †Chimeric antibodies were murine kappa variable region and human IgG1 constant region.

	Antibody Information			Cell Line	
Antibody	**Species**	**Isotype**	**Target**	**M14**	**SW620**
m3F8	Murine	mu. IgG3	GD2	+	-
ch3F8	Chimeric†	hu. IgG1	GD2	+	-
gl_ch3F8	Chimeric†	hu. IgG1	GD2	+	-
ch14.18	Chimeric†	hu. IgG1	GD2	+	-
gl_ch14.18	Chimeric†	hu. IgG1	GD2	+	-
HE195	Mouse	mu. IgM	Blood Group A	-	+

Table S4, related to Figure 5: Summative analysis of RMS-fluctuation (Å) values for germline and affinity mature 3F8 antibodies.

	Light Chain		Heavy Chain	
Antibody Region	**Mature**	**Germline**	**Mature**	**Germline**
FR1	13.7738	18.7409	15.9469	15.9436
CDR1	8.1608	7.3354	2.4234	2.2932
FR2	8.6708	8.4387	7.2653	7.739
CDR2	4.0787	3.5879	8.2772	8.2451
FR3	16.7365	16.6001	14.3388	13.9545
CDR3	3.9913	3.8185	10.6068	8.3091
FR4	8.0108	6.6381	5.3315	5.3012
Total	63.4227	65.1596	64.1899	61.7857
Sum CDRs	16.2308	14.7418	21.3074	18.8474

Supplementary Experimental Procedures

Assignment of putative germline genes

To facilitate comparisons of our work with previous work on immunological evolution of antibodies, we used the same methodology as prior studies to assign the putative germline genes. First, we used both NCBI-BLAST and IMGT/V-Quest alignment algorithms to align 3F8 and ch14.18 heavy and light chains with potential germline genes.

Ch14.18 had 97% nucleotide similarity for the light chain and 92% similarity for the heavy chain nucleotide sequences. These alignments resulted in 2 mutations of the light chain variable region and 19 within the heavy chain. Interestingly, the majority of these heavy chain mutations (12 mutations) fall within the framework regions (FRs) of the variable gene, as opposed to CDRs.

Antibody 3F8 demonstrated a greater degree of similarity between germline and affinity mature sequences. Nucleotide alignments were 97% similar for both the light and heavy chain nucleotide sequences. These alignments indicated the presence of 5 germline mutations of the light chain variable region, as well as 6 mutations of the heavy chain germline region. Interestingly, only one of these mutations (HC: S56I) was hypothesized, by molecular modeling, to be a residue implicated in antigen binding (Ahmed, et al., 2013).

We followed previously used methods for assigning the CDR3 regions of the heavy chains. This region, wherein V-D-J gene recombination occurs, can include some nucleotide insertions/deletions in the V-D and D-J junctions, and in some cases, the D gene can be too short to assign. The standard approach in the field for assigning germline sequences in this region is to align the best germline V, D, and J genes and then leave any nucleotide insertions unchanged relative to the affinity matured antibody. We followed this same approach in the assignment of the germline sequences of 3F8 and ch14.18. Some additional details are described below.

In the analysis of the putative germline of 3F8, the heavy chain protein segment from Thr87 to Thr107 encompasses CDR3. The N-terminal portion of this segment, from Thr87 to Ser94, is encoded by the end of the V-gene segment and reveals 100% nucleotide homology between the germline and mature sequences. The C-terminal portion of this segment, from Ala100B to The107, is encoded by the beginning of the J-gene. There is a single nucleotide mismatch within this region, resulting in a Met-to-Leu mutation at residue 100C. We additionally found that the 'YAMDY' portion of the segment, which represent the D-J junction, is common amongst many immunoglobulins and has 100% homology with their respective D- and J-genes, making this D-J junction assignment highly plausible. Next, the 'HYG' portion of this segment aligns with 100% nucleotide homology to our predicted D-gene and therefore highly plausible. The remainder of the protein segment, an 'RGG' section, could not be defined by nucleotide alignment. However, by performing the BLASTp alignment of the germline with this section, we found that 'RGG' portions immediately following the V-gene are fairly commonplace.

The BLASTp analysis of the putative germline CDR3 of the heavy chain of 14.18 was carried out in a manner identical to that of the previously described 3F8. In this case, the heavy chain CDR3 was markedly smaller and simpler to analyze. A segment of the heavy chain from Ser91 to Thr107 was analyzed. The N-terminal portion from Ser91 to Ser98 is encoded by the end of the V-gene. A single nucleotide mismatch was identified which resulted in an A-to-V mutation at residue 97. The C-terminal portion of the segment, from Met100 to Thr107 is encoded for by the beginning of the J-gene. A single nucleotide mismatch was identified that resulted in a D-to-E mutation at residue 101. The amino acid at position 99 was left unchanged in the putative germline sequence.

Preparation of plasmids

Nucleotide sequences of the affinity mature anti-GD2 antibodies 3F8 and ch14.18 were obtained from previously published literature and patents. Putative germline assignments were made using NCBI-BLAST and IMGT/V-QUEST; in all cases, NCBI-BLAST and IMGT/V-QUEST were in agreement on the top alignments.

DNA encoding for the light and heavy chain variable region inserts were commercially synthesized into pUC57 plasmids with ampicillin resistance (Genscript) and amplified by standard bacterial expansion. Light chain DNA inserts were cut from the plasmid via designed 5'-AgeI and 3'-BsiWI restriction endonuclease sites. Heavy chain inserts were cut via 5'-EcoRI and 3'-NheI sites. Inserts were isolated and purified via standard agarose gel electrophoresis and gel extraction techniques.

Light and heavy chain variable region inserts were ligated into the commercially available pFuse2-CLIg-hk and pFuse-CHIg-hG1 (Invivogen) vectors using T4 DNA ligase (New England BioLabs). Ligation of DNA inserts was validated by colony polymerase chain reaction; primer list available in Table S1.

Transfection into mammalian cells and clonal selection

HEK293 were seeded into a 96-well plate such that their density would be approximately 70% the following day. Prior to transfection, cells were briefly washed with DPBS then Opti-MEM was added. Appropriately paired light and heavy chain plasmids were co-transfected, in a 3:2 ratio, into cells using Lipofectamine 3000 transfection reagent (Life Technologies). Following incubation with transfection reagent, cells were detached from the 96-well plate and washed and re-plated under antibiotic pressure; blasticidin and zeocin resistance are encoded for in the pFuse2-

CLIg-hk and pFuse-CHIg-hG1 plasmids respectively. Clones with continued growth were selected and expanded. Stable cell lines were maintained in DMEM media supplemented with 10% fetal bovine serum (FBS)(ATCC; Manassas, VA) and Media Supplement A (AbCam; Cambridge, MA).

Validation of antibody purity

Polyacrylamide gel electrophoresis. Antibodies purified by protein L affinity chromatography were analyzed by polyacrylamide gel electrophoresis to determine overall purity. 3F8 and 14.18 antibodies, germline and mature, were mixed with NuPage LDS Sample Buffer(4X) (Invitrogen, Carlsbad, CA). Reduced samples were also mixed with NuPage Sample Reducing Agent(10X) (Invitrogen, Carlsbad, CA). Native and reduced samples were loaded into a Bolt 4-12% Bis-Tris Plus gel and run for 45 mins at 150V with 1X MES SDS running buffer. At completion, the gel was stained at room temperature in Coomassie Blue for 2 hrs with gentle shaking. Following staining, Coomassie Blue solution was carefully discarded and the gel was destained with distilled water over approximately 24 hrs with multiple distilled water changes. Once the gel was adequately destained, the gel was imaged using ImageQuant LAS4000 (GE Healthcare Life Sciences, Marlborough, MA).

Size exclusion chromatography. Purified antibodies were further analyzed by size exclusion chromatography high pressure liquid chromatography (SEC HPLC) to validate antibody purity and the absence of antibody aggregates. A TOSOH TSKgel G3000SWxl column (Tosoh Biosciences, King of Prussia, PA) was connected to an Aglient 1200 Series HPLC system (Agilent, Santa Clara, CA). Samples were run in 0.1M phosphate, 0.1M sodium sulfate, 0.05% sodium azide aqueous running buffer at a flow rate of 1 mL/min. Control samples of 3% bovine serum

albumin, purified human IgM (Sigma Aldrich, St. Louis, MO), and purified human IgG (Sigma Aldrich, St. Louis, MO) were run as controls to determine expected elution times.

Microarray fabrication, assay, and analysis

Array fabrication. Carbohydrates to be printed to the array were first conjugated to BSA or HSA to produce neoglycoproteins, carbohydrates covalently linked to proteins by non-naturally occurring linkage. The average number of glycan molecules per molecule of carrier protein was determined by MALDI-MS analysis. Most glycans studied in these analyses were conjugated to the carrier protein at multiple densities (average number of glycans/protein carrier). Full details of the preparation and characterization of the neoglycoproteins has been previously published (Zhang and Gildersleeve, 2012).

Fabrication of the glycan array followed previously reported methods (Campbell, et al., 2010) with the addition of the free acid of DyLight^{TM}649 (0.7 ug/mL, ThermoScientific), a washable fluorescent dye, to the print buffer. This dye was added as an indicator of successful spotting and spot morphology. Array components were printed onto epoxide-coated slides (SuperEpoxy2; ArrayIt; Sunnyvale CA) using a MicroGrid II arrayer (Genomic Solutions; Ann Arbor, MI). 946 Microspotting Pins (ArrayIt; Sunnyvale, CA) were used for this print. Humidity level was maintained at ~50% in the arraying chamber to minimize evaporation during the print. The printing spot size was ~60 μm. Following print completion, printed slides were vacuum sealed stored at -20 °C until use.

Quality of the printed slides was evaluated by testing representative slides from the batch. First, three slides from the batch (one early, one mid, and one late print slide) were scanned using an InnoScan 1100 AL Fluorescence Scanner (Innopsys; Chicago, IL) to detect printing defects.

One slide was then tested against a set of lectins (ConA, WGA, and HPA) and a mouse anti-blood group A antibody. Values from the quality control slide were compared against expected values for a well printed slide.

Binding assay. Prior to experimentation, the sealed slides were brought to room temperature before opening to minimize the formation of condensation on the slide surface. Slides were pre-scanned to determine slide specific defects. An example of the prescan is shown in Figure S3. Next, a 16-well module (Grace Bio-Lab; Bend, OR) was set to the slide, creating 16 independent array wells. 200 μL of blocking reagent (3% w/v BSA in PBS) was added to each well. Blocking was performed overnight at 4 °C. Blocking reagent was then removed and the slides were washed 6 times with PBST (0.05% v/v Tween-20). Recombinantly expressed antibodies were serially diluted in primary incubation buffer, 3% bovine serum albumin (BSA, Sigma) and 1% human serum albumin (HSA, Sigma) in PBST. Each experiment was carried out in duplicate. 50 μL of each dilution was added into a single well on the slide. Each slide also tested a positive control well, human serum diluted 1:50 in primary incubation buffer, and a negative control well, primary incubation buffer only. Slides were incubated at 37 °C for 4 hours with gentle shaking (100 RPM). Following primary incubation, the samples were discarded and slides were washed 6 times with PBST. Antibodies bound to the slide were detected using DyLight^{TM}549-conjugated goat anti-human IgG (Jackson ImmunoResearch Laboratories; West Grove, PA). DyLight^{TM}649-conjugated goat anti-human IgM (Jackson ImmunoResearch Laboratories) was also used to detect human IgM control spots printed to the array, as well as IgM antibodies in the human serum, positive control well. The fluorescently-labelled secondary reagents were diluted 1:500 in secondary incubation buffer, 3% HSA and 1%BSA in PBS, and

added to each well (50 µL/well). Secondary incubation occurred in the dark over 2 hours at 37 °C and 100 RPM. Following incubation, secondary reagent was discarded and slides were washed 6 times with PBST. The slide was then removed from the 16-well module and submerged in PBST for 5 min. Slides were dried by centrifugation at 1000 RPM for 5 min.

Scanning and data analysis. Slides were scanned at 5 µm resolution and 20 linespeed with an InnoScan 1100 AL fluoresence scanner (Innopsys; Chicago, IL). Images were analyzed with GenePix Pro 7.0 software (Molecular Devices Corporation; Sunnyvale, CA). GAL files specific to the array number were aligned with slide component. Print defects (e.g. missing spots) were flagged and excluded from analysis. A background-corrected median fluorescent intensity of 150 was set as the baseline; spots with median intensity less than 150 were considered too low to be accurately measured and were set to 150 (no binding). The final intensity value for an antibody-neoglycoprotein interaction was calculated from the average of duplicate spots in each replicate well.

Human proteome assay and analysis

HuProt v2.0 slides were purchased from CDI Labs (Baltimore, MD). A full list of protein array components can be found on their website (cdi-labs.com). Prior to experimentation, the slides were gently brought to room temperature. To the bottom of the slides, multiple spots of GD2-neoglycoprotein were manually printed; these spots were added to the array to serve as positive control spots. Slides were blocked in blocking buffer (3% w/v BSA in PBS) overnight at 4°C. Blocking buffer was removed and slides were washed 4 times by 5 min submersion in PBST. A LiftSlip (ArrayIt; Sunnyvale, CA) coverslip was carefully fixed atop the HuProt array. Next,

75 μL of sample was carefully applied to the slide. Samples were diluted in incubation buffer (3% BSA and 1% HSA in PBST) to a final concentration of 50 nM for affinity mature ch3F8 and 500 nM for germline ch3F8. Negative control slides were run in the absence of primary antibody with incubation buffer only. Primary incubation was performed at 37 °C for 4 h. Following incubation, LiftSlips were carefully removed and slides were washed 4 times by 5 min submersion in PBST. DyLight™549-conjugated goat anti-human IgG was diluted 1:500 in secondary incubation buffer (3% HSA and 1% BSA in PBS). LiftSlips were refixed to the slide and 75 μL of secondary reagent was added to the slide. Secondary incubation occurred over 2 h at 37 °C in the dark. After incubation, LiftSlips were removed and slides were washed 4 times by 5 min submersion in PBST. Slides were dried by centrifugation at 1000 RPM for 5 min.

Slides were scanned in a manner identical to that of the glycan arrays. GAL files specific to the HuProt v2.0 array were provided by CDI Labs. Examples of full slide scans and subarray images are shown in Figure S8.

Live cell binding and imaging

Cells were washed and plated into flat, clear bottom 96-well plates. Following 24-hour incubation at 37°C and 5% CO_2, germline and affinity mature 3F8 antibodies were added to distinct triplicates of wells. Control wells received RPMI1640 alone. Plates were incubated for 4 h at 37°C and 5% CO_2. Following incubation, plates were gently washed with PBS. RPMI media with DyLight™549-conjugated goat anti-human IgG secondary reagent was added to all wells and plates were incubated for an additional 2 h. Plates were then gently washed with PBS. DAPI counterstain was added to all wells and plates were incubated for 15 minutes. Plates were washed with PBS and imaged using an EVOS FL Auto cell imaging system (Invitrogen; Carlsbad, CA).

Cell fixation, binding, imaging, and flow cytometry

Cells were dissociated from flask surface using trypsin and washed three times in Dulbecco's phosphate buffered saline (DPBS). Following the final wash, cells were pelleted by centrifugation at 250 rcf and suspended in cold 4% paraformaldehyde for 20 minutes. Cells were subsequently pelleted by centrifugation at 250 rcf and washed an additional three times with DPBS. Cells were blocked with 3% BSA in DPBS solution overnight at 4°C.

Following blocking, cells were washed once with DPBS and counted using a TC20 automated cell counter (Bio-Rad, Hercules, CA). Cells were suspended in 3% BSA in DPBS solution to a final cell density of 5 million cells/mL. For one set of independent experiments, purified anti-GD2 antibody (germline 3F8, mature 3F8, germline 14.18, or mature 14.18) was added to distinct duplicates of 0.5 million cells (100 µL of suspension). For a second set of independent experiments, 1 µg of an anti-blood group A antibody, HE-195 (murine IgM; GeneTex, Irvine, CA), was added to distinct duplicates of cells. For a third set of independent experiments, purified anti-GD2 antibody (mature 3F8 or germline 3F8) and anti-blood group A antibody HE-195 were both added to cells. Control sets of cells for all experiments received no primary antibody. Primary binding occurred overnight at 4°C. Each set of experiments was performed in duplicate.

Following primary binding, cells were washed 3 times and suspended in 100 µL 3% BSA in DPBS solution. Cy2-conjugated goat anti-human IgG and Dylight649-conjugated goat anti-mouse IgM secondary antibodies were added all sets of cells. Cells were incubated for 1 hr at 37°C. Following incubation, cells were washed 3 times and suspended in 500 µL 3% BSA in DPBS solution. 10 µL of samples were added to 90 µL added to 3% BSA in DPBS solution with

DAPI counterstain. Samples were added to a flat, clear bottom 96-well plate and imaged using an EVOS FL Auto cell imaging system (Invitrogen; Carlsbad, CA).

The remainder of cells were used for flow cytometry analyses. Samples were analysed using a BD FACSCalibur cell sorting system with a 488 nm blue laser and 635 nm red diode. Control samples, which received secondary antibodies but no primary antibodies, were used as negative controls. Each set of samples was run in duplicate. Positive samples were identified as those with a fluorescence greater than 4 times the average negative control fluorescence.

Molecular dynamics

The crystal structure of the affinity mature antigen binding fragment of 3F8 (PDB ID 3VFG) at 1.65 Å resolution has been previously reported (Ahmed, et al., 2013). This structure is missing coordinates for residues 129-130 in the heavy chain, a loop region that is commonly disordered. We replaced this loop (residues 127-137) with the backbone of the equivalent loop (residues 135-145) from the Tau5 antibody Fab fragment (unpublished; PDB ID 4TQE) which has a very similar conformation. The sequence of the new loop was then converted to that of 3F8 by adding sidechains. A homology model for the germline antibody was made by back-mutating the set of 11 residues that are changed in the maturation process, while preserving the backbone and $\chi 1$ angles to the extent possible. In some cases the positions of surrounding residues were adjusted slightly by hand where necessary (with mutations HC L63 and M106, LC Y50 and D69) to accommodate the sequence change.

The affinity mature and germline structures were read into LeAP in preparation for simulation with Amber 15 (Case, et al., 2015). Hydrogens were added and crystal waters were deleted. All histidines were protonated on Nε. The five disulfide crosslinks between HC 22-92

and 140-195, LC 23-88 and 134-194, and HC 128 - LC 214 were specified. Both structures were minimized in vacuum using the ff14SB forcefield (Maier, et al., 2015) for 100 steps of steepest descent followed by 400 steps of conjugate gradient minimization. Four copies of each structure were then set up in isometric truncated octahedron solvent boxes of TIP3P water. Chloride counter ions were added in positions at least 10 Å apart (replacing randomly chosen water molecules) to neutralize each system. The solvent and ions were minimized for 500 steps with protein atoms strongly restrained with a harmonic force constant of 500 kcal/mol.

Each system was heated from 50K to 300K over 100 ps, with starting atomic velocities assigned differently and randomly for each system copy. Molecular dynamics was run at constant volume and constant temperature using Langevin temperature equilibration with collision frequency $\gamma = 3.0$, and a timestep of 2 fs. Bonds to hydrogen were constrained using SHAKE. Particle Mesh Ewald was used for calculating electrostatic energies with a grid spacing of ~1 Å and a non-bonded cutoff of 10 Å. Protein atoms were again restrained with a harmonic force constant of 100 kcal/mol. After heating, the systems were equilibrated for 200 ps at a constant temperature of 300K using Langevin temperature coupling as before, and constant pressure using the Berendsen barostat with a pressure relaxation time $\tau = 2.0$ ps. Restraints on the protein atoms were relaxed stepwise from 25 to 10 kcal/mol. Production molecular dynamics was run in the NPT ensemble as above with no restraints. Frames were saved every 2 ps (2000 steps). We used the pmemd.cuda implementation of sander (Le Grand, et al., 2013), run on a single GPU, for a total simulation time of 30 ns for each system copy.

The RMS distance from the starting conformation over time was calculated for the backbone atoms of each domain (VL, CL, VH, and CH1) in each system copy using cpptraj (Roe and Cheatham, 2013). This was used to assess system stability and equilibration, and is shown in

Figure S13. The last 25 ns of each simulation was used for further data analysis, to give a total of 100 ns of data across the four copies of the affinity mature and germline structures. RMS atomic fluctuations, shown in Figures S14, were calculated by first overlaying and averaging the backbone atom coordinates of each domain. Each frame was then RMS fit to this average structure and the mass-weighted average of the backbone atom fluctuations was calculated for each residue. The statistical significance of RMSF differences between affinity mature and germline residues could be calculated due to the four independent simulation copies for each structure using the Wilcoxon rank sum test to a maximum significance level of $p = 0.01$ (Likic, et al., 2005). Crystallographic B-factors from 3VFG were averaged over the backbone atoms for each residue and converted to RMS fluctuations using the equation $U_i = \mathrm{sqrt}(3B_i/8\pi^2)$.

For the worm plots (Figure 5a and 5b) the RMS fluctuations were calculated slightly differently, with the alignment for the average structure calculation and the RMS fit to the average structure using only the backbone atoms of the core β-sheet residues in the variable domains: HC residues 4-7, 11-12, 18-24, 34-39, 46-51, 57-59, 67-72, 77-82, 91-97, 108-109, and 113-117; LC residues 4-7, 10-14, 19-25, 34-38, 45-49, 53-54, 62-66, 84-89, and 99-104. The worm plots were rendered in UCSF Chimera (Pettersen, et al., 2004) by assigning the mass-weighted RMSF average to each residue as an attribute, and mapping it to the radius/fatness of the backbone ribbon. Loop RMSD histograms (Figure 5c-h) were generated in cpptraj (Roe and Cheatham, 2013) by calculating the RMS distance of the residues in each CDR loop (H1 = 26-33, H2 = 52-56, H3 = 95-101, L1 = 26-33, L2 = 50-61, L3 = 90-101) from the starting conformation over time. The RMSD values were binned into histograms with a minimum RMSD of 0 Å, a maximum of 5 Å, and a step size of 0.2 Å. Bin populations were normalized so that the sum over all bins was equal to 1.

The molecular hydrophobic potential was calculated based on the surface projection of atomic logP values (Ghose, et al., 1998; Steinkellner, et al., 2009), along with the surface electrostatic potential using DelPhi (Nicholls et al., 1991). Surfaces were rendered in PyMol (Delano, 2002).

References

Ahmed, M., Goldgur, Y., Hu, J., Guo, H.F., and Cheung, N.K. (2013). In silico driven redesign of a clinically relevant antibody for the treatment of GD2 positive tumors. PLoS One *8*, e63359.

Campbell, C.T., Zhang, Y., and Gildersleeve, J.C. (2010). Construction and use of glycan microarrays. Curr. Protoc. Chem. Biol. *2*, 37-53.

Case, D.A., Berryman, J.T., Betz, R.M., Cerutti, D.S., T.E. Cheatham, I., Darden, T.A., Duke, R.E., Giese, T.J., Gohlke, H., Goetz, A.W., et al. (2015). AMBER 2015. (University of California, San Francisco.

Cheung, N.K., Guo, H., Hu, J., Tassev, D.V., and Cheung, I.Y. (2012). Humanizing murine IgG3 anti-GD2 antibody m3F8 substantially improves antibody-dependent cell-mediated cytotoxicity while retaining targeting in vivo. Oncoimmunology *1*, 477-486.

Delano, WL. The PyMOL molecular graphics system. Version 0.99

Le Grand, S., Gotz, A.W., and Walker, R.C. (2013). SPFP: Speed without compromise-A mixed precision model for GPU accelerated molecular dynamics simulations. Comput. Phys. Commun. *184*, 374-380.

Likic, V.A., Gooley, P.R., Speed, T.P., and Strehler, E.E. (2005). A statistical approach to the interpretation of molecular dynamics simulations of calmodulin equilibrium dynamics. Protein Sci. *14*, 2955-2963.

Maier, J.A., Martinez, C., Kasavajhala, K., Wickstrom, L., Hauser, K.E., and Simmerling, C. (2015). ff14SB: Improving the Accuracy of Protein Side Chain and Backbone Parameters from ff99SB. J. Chem. Theory Comput. *11*, 3696-3713.

Nicholls, A., and Honig, B. (1991) A rapid finite difference algorithm, utilizing successive over-relaxation to solve the Poisson-Boltzmann equation. J. Comput. Chem. *12*, 435-445.

Pettersen, E.F., Goddard, T.D., Huang, C.C., Couch, G.S., Greenblatt, D.M., Meng, E.C., and Ferrin, T.E. (2004). UCSF Chimera--a visualization system for exploratory research and analysis. J. Comput. Chem. *25*, 1605-1612.

Roe, D.R., and Cheatham, T.E., 3rd. (2013). PTRAJ and CPPTRAJ: Software for Processing and Analysis of Molecular Dynamics Trajectory Data. J. Chem. Theory Comput. *9*, 3084-3095.

Steinkeller, G., Rader, R., Thallinger, G.G., Kratky, C., and Gruber, K. (2009) VASCo: computation and visualization of annotate protein surface contacts. BMC Bioinformatics *10*, 32.

Zhang, Y., and Gildersleeve, J.C. (2012). General procedure for the synthesis of neoglycoproteins and immobilization on epoxide-modified glass slides. Methods Mol. Biol. *808*, 155-165.